REPORT DOCUMENTATION PAGE

Form Approved
OMB No. 0704-0188

1. REPORT DATE *(DD-MM-YYYY)*	**2. REPORT TYPE**	**3. DATES COVERED** *(From - To)*
17-11-2009	Journal Article	

4. TITLE AND SUBTITLE

The Syntheses and Structure of the First Vanadium(IV) and Vanadium(V) Binary Azides, $V(N_3)_4$, $[V(N_3)_6]^{2-}$ and $[V(N_3)_6]^-$ (PREPRINT)

5a. CONTRACT NUMBER

5b. GRANT NUMBER

5c. PROGRAM ELEMENT NUMBER

6. AUTHOR(S)
Ralf Haiges and Karl O. Christe (USC); Jerry A. Boatz(AFRL/RZSP)

5d. PROJECT NUMBER

5e. TASK NUMBER

5f. WORK UNIT NUMBER
50260541

7. PERFORMING ORGANIZATION NAME(S) AND ADDRESS(ES)

Air Force Research Laboratory (AFMC)
AFRL/RZSP
10 E. Saturn Blvd.
Edwards AFB CA 93524-7680

8. PERFORMING ORGANIZATION REPORT NUMBER

AFRL-RZ-ED-JA-2009-434

9. SPONSORING / MONITORING AGENCY NAME(S) AND ADDRESS(ES)

Air Force Research Laboratory (AFMC)
AFRL/RZS
5 Pollux Drive
Edwards AFB CA 93524-7048

10. SPONSOR/MONITOR'S ACRONYM(S)

11. SPONSOR/MONITOR'S NUMBER(S)
AFRL-RZ-ED-JA-2009-434

12. DISTRIBUTION / AVAILABILITY STATEMENT

Approved for public release; distribution unlimited (PA #10005).

13. SUPPLEMENTARY NOTES
For publication in Angewandte Chemie Journal

14. ABSTRACT

During the last decade, there has been much interest in inorganic polyazide chemistry.[1-16] Because of the energetic nature of the azido group, polyazides are highly endothermic compounds, whose energy content increases with an increasing number of azido ligands. It is, therefore, not surprising, that the synthesis of molecules with a high number of azido groups is very challenging due to their explosive nature and shock-sensitivity.

15. SUBJECT TERMS

16. SECURITY CLASSIFICATION OF:			**17. LIMITATION OF ABSTRACT**	**18. NUMBER OF PAGES**	**19a. NAME OF RESPONSIBLE PERSON**
					Dr. Jerry Boatz
a. REPORT	**b. ABSTRACT**	**c. THIS PAGE**			**19b. TELEPHONE NUMBER** *(include area code)*
Unclassified	**Unclassified**	**Unclassified**	SAR	36	N/A

The Syntheses and Structure of the First Vanadium(IV) and Vanadium(V) Binary Azides, $V(N_3)_4$, $[V(N_3)_6]^{2-}$ and $[V(N_3)_6]^-$ ** (PREPRINT)

Ralf Haiges, Jerry A. Boatz, and Karl O. Christe**

Dedicated to the memory of Prof. Robert Bau

During the last decade, there has been much interest in inorganic polyazide chemistry.[1-16] Because of the energetic nature of the azido group, polyazides are highly endothermic compounds, whose energy content increases with an increasing number of azido ligands. It is, therefore, not surprising, that the synthesis of molecules with a high number of azido groups is very challenging due to their explosive nature and shock-sensitivity.

Although a significant number of pentavalent binary azido compounds of the heavier elements of Group V, i.e., niobium and tantalum, have been prepared and characterized.[14,15], the situation is different for vanadium for which only trivalent binary azides were known.[17,18] For the higher oxidation states of vanadium, only tertiary

---

[*] Dr. R. Haiges, Prof. Dr. K. O. Christe
Loker Research Institute and Department of Chemistry
University of Southern California
Los Angeles, CA 90089-1661 (USA)
Fax: (+1) 213-740-6679
E-mail: haiges@usc.edu, kchriste@usc.edu
Dr. J. A. Boatz
Space and Missile Propulsion Division
Air Force Research Laboratory (AFRL/RZSP)
10 East Saturn Boulevard
Edwards Air Force Base, CA 93524 (USA)

[**] This work was funded by the Air Force Office of Scientific Research, the Office of Naval Research, the Defense Threat Reduction Agency, and the National Science Foundation. We thank Profs. G. Olah and S. Prakash for their steady support, and Drs. W. Wilson and R. Wagner for their help and stimulating discussions. Grants of computer time from the Department of Defense High Performance Computing Modernization Program at the Engineer Research and Development (ERDC) and Navy Department of Defense Supercomputing Centers are gratefully acknowledged.

or quartenerary azides, such as $VOCl_2N_3$,[19] $[VO(N_3)_4]^{2-}$,[18,20,21] and $[V(N_3)_3(N_3S_2)]^{2-}$,[22] have been reported, and no binary vanadium(V) compounds had been known except for VF_5, VF_6^- and V_2O_5.

By analogy with our previous syntheses of binary azides,[14] vanadium fluorides were reacted with an excess of Me_3SiN_3 in acetonitrile solution. This resulted in complete fluoride-azide exchange. In the case of VF_4, a dark red, almost black solution of $V(N_3)_4$ [Eq. (1)] was obtained.

$$VF_4 + 4\,Me_3SiN_3 \xrightarrow{CH_3CN} V(N_3)_4 + 4\,Me_3SiF \qquad (1)$$

As expected for a covalently bonded polyazide,[23] solid $V(N_3)_4$ is very shock-sensitive. It can explode violently upon the slightest provocation, e.g., when either touched with a spatula or by a rapid change in temperature. All attempts to obtain single crystals of $V(N_3)_4$ by recrystallization were unsuccessful. The identity of the vanadium tetraazide was established by the observed material balance, its low-temperature Raman spectrum, and by its conversion with $Ph_4P^+N_3^-$ into the $[Ph_4P^+]_2[V(N_3)_6]^{2-}$ salt which was characterized by its crystal structure. The recording of the Raman spectrum of $V(N_3)_4$ was very challenging due to the black color of the sample, its amorphism and extreme shock-sensitivity. In spite of these difficulties we succeeded to record several reproducible Raman spectra of amorphous samples and one spectrum of a crystalline sample before it exploded. In Table 1, the vibrational frequencies and intensities observed for the amorphous samples are compared with those calculated for the free molecular species at the MP2/MCP-TZP level of theory. The vibrational frequencies calculated for $V(N_3)_4$ at the B3LYP/MCP-TZP level

are given as Table S1 in the Supplementary Material. Table 1 shows very good agreement between the calculated and observed frequencies suggesting that amorphous $V(N_3)_4$ is only weakly associated. In contrast, the Raman spectrum obtained for the crystalline sample (given as footnote [a] in Table 1) deviated significantly from that of the amorphous sample. It showed three intense bands in the region of the V-N stretching modes, indicating association.

The MP2 calculations resulted in a minimum energy structure of S_4 symmetry, while the B3LYP calculation favored a D_{2d} structure (Table 2). Both structures are very similar and can be derived from tetrahedral VN_4 skeletons in which two of the bond angles are slightly compressed while the other four are widened. However, there is a difference in the arrangement of the azido ligands. Generally, in S_n-type structures, the azido ligands are arranged in a propeller-type fashion, while in D_{nd}-type structures the presence of an additional mirror plane along the *n*-fold inversion axes forces the azido ligands into arrangements which are symmetric to this plane. In view of the complexity of the spectra, their low sensitivity to minor rearrangements of the ligands and experimental difficulties in obtaining high resolution data, the observed spectra do not always allow a clear distinction between different geometries. However, it appears that generally the propeller-type ligand arrangements of S_n symmetry are favored over the D_{nd} structures and, therefore, the S_4 structure is preferred by us for $V(N_3)_4$.

As found for other neutral binary polyazides,[8-15] $V(N_3)_4$ can also be stabilized by anion formation which increases the ionicity of the azido group. Because an ionic azide group possesses two double bonds while a covalent azide group has a single and a triple bond, increasing the ionicity of an azido ligand enhances the activation energy barrier

toward N_2 elimination. Accordingly, the hexaazidovanadate anion $[V(N_3)_6]^{2-}$ was prepared by the reaction of the tetraazide with two equivalents of PPh_4N_3 in acetonitrile solution [Eq. (2)].

$$V(N_3)_4 + 2\,[PPh_4]N_3 \xrightarrow{CH_3CN} [PPh_4]_2[V(N_3)_6] \qquad (2)$$

The resulting $[PPh_4]_2[V(N_3)_6]$ was isolated as a room-temperature stable, crystalline black solid. Because of the increased ionicity of its azido ligands and the presence of two large counter-ions per anion, it is much less sensitive and explosive than $V(N_3)_4$.

The $[PPh_4]_2[V(N_3)_6]$ salt was characterized by the observed material balance, its IR and Raman spectra (Experimental Section and Figure S1 and Table S2 of the Supplementary Material), and its crystal structure.[24] The theoretical calculations predict two possible structures of very similar energy, having C_i and D_{3d} symmetry, respectively, (see Table 2). The C_i structure is a slightly distorted, propeller-type S_6 structure. At the B3LYP/MCP-TZP level, it is favored by 4.2 kcal/mol over the D_{3d} structure. However, at the MP2/MCP-TZP level of theory, the D_{3d} structure is slightly lower in energy by 0.9 kcal/mol. In view of their small energy differences and sensitivity to the level of theory used, the theoretical predictions do not allow the reliable prediction of a preferred structure, even for the free gaseous species. In the solid state, small differences in packing energies and the influence of different counter ions could further contribute to this problem. Since the crystal structure analysis established for the $P(Ph_4)^+$ salt the C_i structure,[24] assignments of the observed vibrational spectra to individual modes were made for this isomer by comparison with the calculated spectra and resulted in very good agreement (Table S2, Supplementary Material). The calculated vibrational spectra of the D_{3d} isomer are given as Table S3 in the Supplementary Material.

The structure of $[PPh_4]_2[V(N_3)_6]$ was established by a single crystal X-ray diffraction study (Figure 2 and Tables S4 through S8). The X-ray crystal structure of the $[PPh_4]_2[V(N_3)_6]$ salt[24] revealed the presence of well separated $[PPh_4]^+$ and $[V(N_3)_6]^{2-}$ ions. The closest V···N and N···N contacts between neighboring anions are 7.1 Å and 4.6 Å, respectively. The geometry of the $[V(N_3)_6]^{2-}$ anion is only slightly distorted from perfect S_6 symmetry and is in good agreement with the propeller-type C_i structure predicted by our theoretical calculations and the ones previously found for the similar hexaazides $[As(N_3)_6]^-$,[6,23] $[Sb(N_3)_6]^-$,[11] $[Si(N_3)_6]^{2-}$,[4] $[Ge(N_3)_6]^{2-}$,[3] $[Nb(N_3)_6]^-$,[14] $[Ta(N_3)_6]^-$,[14] $W(N_3)_6$,[13] $[Ti(N_3)_6]^{2-}$,[12] and $[Se(N_3)_6]^{2-}$,[25] but contrary to that of $[Te(N_3)_6]^{2-}$[7] in which the free valence electron pair on Te becomes sterically active.

The structure of the $[V(N_3)_6]^{2-}$ anion consists of an asymmetric $V(N_3)_3$ unit with three azido groups covalently bonded to the vanadium in a trigonal pyramidal fashion. The remaining three azido groups are generated by symmetry. Selected bond length and angles are listed in Figure 1 and Table S5. The observed average V-N distance of 1.982 Å is shorter than the calculated ones (B3LYP: 2.024 – 2.026 Å, MP2: 2.005 Å) and the observed average V-N distances in $(\eta^5\text{-}C_5H_5)_2V(N_3)_2$ (2.080 Å)[26], $[V(N_3)_3(N_3S_2)]_2^{2-}$ (2.02 Å),[27] and the terminal azido group in $[(\eta^5\text{-}C_5Me_5)VCl(N_3)(\mu\text{-}N_3)]_2$ (2.058 Å),[28] and similar to the observed V-N distance for the terminal azido groups in $[(\eta^5\text{-}C_5Me_5)V(N_3)_2(\mu\text{-}N_3)]_2$ (1.981 Å).[28] The observed V-N distances of the $[V(N_3)_6]^{2-}$ anion are more than 0.05 Å longer than the one calculated for $V(N_3)_4$. This increase in bond length can be explained by the higher ionicity of the V-N bonds in $[V(N_3)_6]^{2-}$, caused by the two formal negative charges. The observed and calculated N-N bond lengths serve as further evidence for the increased ionicity of the azide ligands in $[V(N_3)_6]^{2-}$. The two N-N

distances of the N_3 groups in $V(N_3)_4$ are calculated by B3LYP to differ by 0.098 Å (MP2: 0.053 Å), indicating the presence of predominantly covalent azido groups with strong N_β-N_γ triple bond character. In the $[V(N_3)_6]^{2-}$ anion, the differences in the N-N distances in the azido groups are more similar (B3LYP: 0.049 and 0.044 Å, MP2: 0.023 and 0.021 Å) implying higher ionicity. It should be noted that in the observed crystal structure of $[PPh_4]_2[V(N_3)_6]$ the differences in the N-N distances of the three different azido groups are not identical and vary from 0.085 Å to 0.068 and 0.030 Å, indicating varying degrees of ionicity of the azide ligands. Since the differences in the N-N distances calculated for the free gaseous anion are identical for all three azido ligands, the experimentally observed deviations are attributed to solid state effects.

Our attempts to prepare $V(N_3)_5$ were unsuccessful. Even at a temperature of -35 °C, the reaction of VF_5 with an excess of Me_3SiN_3 in acetonitrile solution resulted in the release of elemental nitrogen and the reduction of V(V) to V(IV), yielding a dark red, almost black solution of $V(N_3)_4$ [Eq. (3)].

$$2\ VF_5 + 10\ Me_3SiN_3 \xrightarrow{CH_3CN} 2\ V(N_3)_4 + 10\ Me_3SiF + 3\ N_2 \qquad (3)$$

Pumping off the volatile compounds at ambient temperature resulted in the isolation of the neat tetra-azide as an amorphous black solid.

However, the preparation of a binary vanadium(V) azide was possible by taking advantage of the fact that the oxidation potential of an anion is lower than that of its neutral parent compound, thus avoiding the reduction of V(+V) to V(+IV) by azide. Using $[NMe_4][VF_6]$ as a starting material and reacting it with an excess of Me_3SiN_3 in acetonitrile

solution resulted in the isolation of the corresponding hexaazidovanadate(V) compound [Eq. (4)].

$$[NMe_4][VF_6] + 6\ Me_3SiN_3 \xrightarrow{CH_3CN} [NMe_4][V(N_3)_6] + 6\ Me_3SiF \qquad (4)$$

$[NMe_4][V(N_3)_6]$ was isolated as a black amorphous solid that is thermally stable at room-temperature but is highly shock-sensitive and explodes violently upon the slightest provocation. Its composition was established by the observed material balance and its low-temperature Raman spectrum (Figure 2). The Raman spectrum of $[V(N_3)_6]^-$ is distinctively different from that of $[V(N_3)_6]^{2-}$. Not only are the antisymmetric N_3 and skeletal V-N stretching vibrations shifted to higher frequencies, as expected for an increased covalency of the azido groups due to the decreased formal negative charge of the anion, but also the band splittings and relative intensities differ significantly. The shift of the bands to higher frequencies with decreasing formal negative charges has previously been demonstrated for the VF_6^-, VF_6^{2-} and VF_6^{3-} series. [29] In $[V(N_3)_6]^{2-}$, the VN_6 skeleton is almost perfectly octahedral and the azido ligands exhibit a propeller type arrangement but differ significantly in their ionic character due to solid state effects. By contrast, the VN_6 skeleton of $[V(N_3)_6]^-$ is significantly distorted from octahedral symmetry (Table 2) with three shorter and three longer V-N bonds in *mer* positions (Δ V-N ~ 0.035 Å at the B3LYP level). The structure can be visualized as being composed of twoT-shaped halves, one possessing the shorter bonds and the other one the longer bonds and the crossbars of the two Ts being orthogonal to each other, forming the equatorial plane of a distorted octahedron. The azido ligands of $[V(N_3)_6]^-$ are more covalent than those in $[V(N_3)_6]^{2-}$ with an average N-N bond difference of 0.052 Å, and do not vary much in their ionic character. The pronounced splittings of the antisymmetric N_3 stretching modes in $[V(N_3)_6]^-$ can

readily be accounted for by the increased distortion of its VN_6 skeleton and the greater variations in its V-N bond lengths and is further supported by the calculated vibrational spectra. The difference in the counter ions (PPh_4^+ versus $N(CH_3)_4^+$), the change in the anion to cation ratios and the presence of some residual CH_3CN in the $[N(CH_3)_4][V(N_3)_6]$ sample are probably only minor contributors to these differences. The observed CH_3CN frequencies are similar to those of the free molecule in the gas phase[30] and differ from those observed for bound CH_3CN in $Nb(N_3)_5(CH_3CN)$ and $Ta(N_3)_5(CH_3CN)$,[14] thus demonstrating that the CH_3CN in our $[N(CH_3)_4][V(N_3)_6]$ sample is not bound as a ligand. The calculated and observed vibrational frequencies and intensities and their assignments are listed in Table 3.

In summary, in this study the first binary vanadium(IV) azides, $V(N_3)_4$ and $[V(N_3)_6]^{2-}$, and vanadium(V) azide, $V(N_3)_6^-$, have been prepared and characterized. The neutral tetraazide and $V(N_3)_6^-$ are stable at ambient temperature but highly explosive. The $[V(N_3)_6]^{2-}$ anion, particularly when combined with a large inert counter ion, is more manageable. Furthermore, the $V(N_3)_6^-$ anion is the first binary vanadium(V) species containing a ligand other than fluorine or oxygen.

Experimental Part

Caution! *The polyazides of this work are extremely shock-sensitive and can explode violently upon the slightest provocation. They should be handled only on a scale of less than 1 mmol using appropriate safety precautions.*[14] ***Ignoring safety precautions can lead to serious injuries!***

Materials and Apparatus

All reactions were carried out in Teflon-FEP ampules that were closed by stainless steel valves. Volatile materials were handled in a Pyrex glass or stainless steel/Teflon-FEP vacuum line.[31] All reaction vessels were passivated with ClF_3 prior to use. Nonvolatile materials were handled in the dry argon atmosphere of a glove box. Raman spectra were recorded directly in the Teflon reactors in the range 4000–80 cm^{-1} on a Bruker Equinox 55 FT-RA spectrophotometer, using a Nd-YAG laser at 1064 nm with power levels of less than 50 mW(!). Infrared spectra were recorded in the range 4000-400 cm^{-1} on a Midac, M Series, FT-IR spectrometer using KBr pellets.

The starting materials VF_5, VF_4 (both Ozark Mahoning) and PPh_4Cl (Aldrich) were used without further purification. $(CH_3)_3SiN_3$ (Aldrich) was purified by fractional condensation prior to use. Solvents were dried by standard methods and freshly distilled prior to use. PPh_4N_3 was obtained from PPh_4Cl by anion-exchange in aqueous solution.[32] $[NMe_4][VF_6]$ was prepared from anhydrous NMe_4F and VF_5 in HF solution.

Preparation of $V(N_3)_4$

Samples of either VF_4 or VF_5 (0.35 mmol) were loaded into a Teflon-FEP ampule, followed by the addition of CH_3CN (50 mmol) and Me_3SiN_3 (4.32 mmol) *in vacuo* at -196 °C. The mixtures were allowed to warm to room temperature and within minutes turned first yellow, then brownish-red and finally black. After 30 min, the temperature was lowered to –20 °C, and all volatile material was pumped off over a period of 8 h, leaving behind black solids. Inspection of the volatile material, trapped at –196 °C, by gas-FTIR spectroscopy showed CH_3CN and $(CH_3)_3SiF$[33,34] as the sole reaction by-product.

Preparation of $[PPh_4]_2[V(N_3)_6]$

$[PPh_4]N_3$ (0.4 mmol) was loaded into a Teflon-FEP ampule containing a frozen solution of $V(N_3)_4$ (0.20 mmol) in CH_3CN (30 mmol) at –78 °C. The mixture was warmed to room temperature, resulting in the formation of a dark solution. After 20 min, the temperature was lowered to –20 °C and all volatile material was slowly pumped off, leaving behind a black, crystalline solid (210 mg; weight expected for 0.20 mmol $[PPh_4]_2[V(N_3)_6]$: 196 mg). The compound was characterized by vibrational spectroscopy (Table S2 and Figure S1) and its crystal structure.

Preparation of $[NMe_4][V(N_3)_6]$

$[NMe_4][VF_6]$ (0.3 mmol) was loaded into a Teflon-FEP ampule, followed by the addition of CH_3CN (50 mmol) and Me_3SiN_3 (2.5 mmol) *in vacuo* at -196 °C. The mixture was allowed to warm to room temperature. Within minutes, the mixture turned black. After 30 min, the temperature was lowered to –20 °C, and all volatile material was pumped off, leaving behind a black solid (125 mg; weight expected for 0.30 mmol $[NMe_4][V(N_3)_6]$: 111 mg). Inspection of the volatile material, trapped at –196 °C, by gas-FTIR spectroscopy showed CH_3CN and $(CH_3)_3SiF$[33,34] as the sole reaction by-product.

Theoretical Methods

All structures were fully optimized using second order perturbation theory (MP2)[35] and density functional theory (DFT) utilizing the B3LYP hybrid functional.[36] A model core potential (MCP) and corresponding valence-only triple zeta basis set[37] was used in all computations. Stationary points were verified as local minima via diagonalization of the mass-weighted hessian. All calculations were performed using the GAMESS[38] quantum chemistry code.

Keywords: Vanadium Azides, Crystal Structures, Vibrational Spectra, Electronic Structure Calculations

References

[1] a) Z. Dori, R. F. Ziolo, *Chem. Rev*. **1973**, *73*, 247; b) I. C. Tornieporth-Oetting, T. M. Klapötke, *Angew. Chem.* **1995**, *107*, 559; *Angew. Chem. Int. Ed.* **1995**, *34*, 511; c) T. M. Klapötke, *Chem. Ber*. **1997**, *130*, 443; d) A. Kornath, *Angew. Chem.* **2001**, *113*, 3231; *Angew. Chem. Int. Ed.* **2001**, *113*, 3135; g) W. Fraenk, T. M. Klapötke in *Inorganic Chemistry Highlights* (Eds.: G. Meyer, D. Naumann, L. Wesemann), Wiley-VCH, Weinheim, **2002**; h) J. Müller, *Coord. Chem. Rev.* **2002**, *235*, 105; i) C. Knapp, J. Passmore, *Angew. Chem.* **2004**, *116*, 4938; *Angew. Chem. Int. Ed.* **2004**, *43*, 4834.

[2] B. Neumüller, F. Schmock, K. Dehnicke, *Z. Anorg. Allg. Chem.* **1999**, *625*, 1243.

[3] A. C. Filippou, P. Portius, D. U. Neumann, K.-D. Wehrstedt, *Angew. Chem.* **2000**, *112*, 4524; *Angew. Chem. Int. Ed*. **2000**, *39*, 4333.

[4] A. C. Filippou, P. Portius, G. Schnakenburg, *J. Am. Chem. Soc.* **2002**, *124*, 12396.

[5] T. M. Klapötke, B. Krumm, P. Mayer, H. Pietrowski, O. P. Ruscitti, A. Schiller, *Inorg. Chem*. **2002**, *41*, 1184.

[6] K. Karaghiosoff, T. M. Klapötke, B. Krumm, H. Nöth, T. Schütt, M. Suter, *Inorg. Chem.* **2002**, *41*, 170.

[7] T. M. Klapötke, B. Krumm, P. Mayer, I. Schwab, *Angew. Chem.* **2003**, *115*, 5824; *Angew. Chem. Int. Ed.* **2003**, *42*, 6024.

[8] R. Haiges, J. A. Boatz, A. Vij, M. Gerken, S. Schneider, T. Schroer, K. O. Christe, *Angew. Chem.* **2003**, *115*, 6027; *Angew. Chem. Int. Ed.* **2003**, *42*, 5847.

[9] R. Haiges, A. Vij, J. A. Boatz, S. Schneider, T. Schroer, M. Gerken, K. O. Christe, *Chem. Eur. J.* **2004**, *10*, 508.

[10] R. Haiges, S. Schneider, T. Schroer, K. O. Christe, *Angew. Chem.* **2004**, *116*, 5027; *Angew. Chem. Int. Ed.* **2004**, *43*, 4919.

[11] R. Haiges, J. A. Boatz, A. Vij, V. Vij, M. Gerken, S. Schneider, T. Schroer, M. Yousufuddin, K. O. Christe, *Angew. Chem. Int. Ed.* **2004**, *43*, 6676.

[12] R. Haiges, J. A. Boatz, S. Schneider, T. Schroer, M. Yousufuddin, K. O. Christe, *Angew. Chem. Int. Ed.* **2004**, *43*, 3148.

[13] R. Haiges, J. A. Boatz, R. Bau, S. Schneider, T. Schroer, M. Yousufuddin, K. O. Christe, *Angew. Chem. Int. Ed.* **2005**, *44*, 1860.

[14] R. Haiges, J. A. Boatz, T. Schroer, M. Yousufuddin, K. O. Christe, *Angew. Chem. Int. Ed.* **2006**, *45*, 4830.

[15] R. Haiges, J. A. Boatz, M. Yousufuddin, K. O. Christe, *Angew. Chem. Int. Ed.* **2007**, *46*, 2869.

[16] a) J. P. Johnson, G. K. MacLean, J. Passmore, P. S. White, *Can. J. Chem.* **1989**, *67*, 1687; b) T. M. Klapötke, B. Krumm, P. Mayer, I. Schwab, *Angew. Chem.* **2003**, *115*, 6024; *Angew. Chem. Int. Ed.* **2003**, *42*, 5843

[17] V. Gutmann, O. Leitmann, A. Scherhaufer, H. Czuba, *Mh. Chem.* **1967**, *98*, 188.

[18] H.-H. Schmidtke, D. Garthoff, *Z. Naturforsch.* **1969**, *24a*, 126.

[19] K. Dehnicke, *J. Inorg. Nucl. Chem*. **1965**, *27*, 809.

[20] W. Beck, W. P. Fehlhammer, P. Pöllmann, E. Schuierer, K. Feldl, *Chem. Ber*. **1967**, *100*, 2335.

[21] W. Beck, E. Schuierer, P. Pöllmann, W. P. Fehlhammer, *Z. Naturforsch.* **1966**, *21b*, 811.

[22] J. Hanich, M. Krestel, U. Mueller, K. Dehnicke, D. Rehder, *Z. Naturforsch.* **1984**, *39b*, 1686.

[23] A. M. Golub, H. Koehler, V. V. Stopenko, *Chemistry of Pseudohalides*, Elsevier, Amsterdam, **1986**.

[24] Crystal data for $C_{48}H_{40}N_{18}P_2V$: M_r = 981.86, triclinic, space group *P*-1, a = 10.098(3), b = 10.365(3), c = 12.258(4) Å, α = 88.498(6), β = 75.688(6), γ = 69.406(6) °, V = 1161.1(7) Å^3, *F(000)* = 507, $\rho_{calcd.}$ (Z = 1) = 1.404 g·cm^{-3}, μ = 0.340 mm^{-1}, approximate crystal dimensions 0.28 x 0.20 x 0.05 mm^3, θ range = 1.72 to 27.59°, $Mo_{K\alpha}$ (λ = 0.71073 Å), T = 143(2) K, 7186 measured data (Bruker 3-circle, SMART APEX CCD with χ-axis fixed at 54.74°, using the SMART V 5.630 program, Bruker AXS: Madison, WI, 2003), of which 5017 (R_{int} = 0.0241) unique. Lorentz and polarization correction (SAINT V 6.45 program, Bruker AXS: Madison, WI, 2003), absorption correction (SADABS program, Bruker AXS: Madison, WI, 2003). Structure solution by Patterson method (SHELXTL 6.14, Bruker AXS: Madison, WI, 2003), full-matrix least-squares refinement on F^2, data to parameters ratio: 16.0 : 1, final *R* indices [$I>2\sigma(I)$]: *R1* = 0.0666, *wR2* = 0.1757, R indices (all data): *R1* = 0.0955, *wR2* = 0.1938, GOF on F^2 = 1.042. Further crystallographic details can be obtained from the Cambridge Crystallographic Data

Centre (CCDC, 12 Union Road, Cambridge CB21EZ, UK (Fax: (+44) 1223-336-033; e-mail: deposit@ccdc.cam.ac.uk) on quoting the deposition no. CCDC 288159.

[25] T. M. Klapötke, H. Nöth, T. Schütt, M. Warchhold, *Angew. Chem.* **2000**, *112*, 2197; *Angew. Chem. Int. Ed.* **2000**, *39*, 2108.

[26] T. M. Klapötke, B. Krumm, M. Scherr, R. Haiges, K. O. Christe, *Angew. Chem.* **2007**, *119*, 8840; *Angew. Chem. Int. Ed.* **2007**, *46*,8686.

[27] J. Honzicek, M. Erben, I. Cisarova, J. Vinklarek, *Appl. Organomet. Chem.* **2005**, *19*, 102.

[28] M. Herberhold, A.-M. Dietel, W. Milius, *Z. Anorg. Allg. Chem*. **1999**, *625*, 1885.

[29] R. Becker, W. Sawodny, *Z. Naturforsch.* **1973**, *28b*, 360.

[30] T. Shimanouchi, *Nat. Stand. Ref. Data Ser. , Nat. Bur. Stand. (U.S.)*, **1972,** *39*, 84.

[31] K. O. Christe, W. W. Wilson, C. J. Schack, R. D. Wilson, *Inorg. Synth.* **1986**, *24*, 39.

[32] R. Haiges, T. Schroer, M. Yousufuddin, K. O. Christe, *Z. Anorg. Allg. Chem.* **2005**, *631*, 2691.

[33] K. Licht, P. Koehler, H. Kriegsmann, *Z. Anorg. Allg. Chem.* **1975**, *415*, 31.

[34] H. Bürger, *Spectrochim. Acta* **1968**, *24A*, 2015.

[35] a) C. Moller, M. S. Plesset, *Phys. Rev.* **1934,** *46*, 618; J. A. Pople, J. S. Binkley, R. Seeger, *Int. J. Quantum Chem.* **1976**, *S10*, 1; b) M. J. Frisch, M. Head-Gordon, J. A. Pople, *Chem.Phys.Lett.* **1990**, *166*, 275; c) J. Bartlett, D. M. Silver, *Int. J. Quantum Chem. Symp.* **1975,** *9*, 1927.

[36] a) A. D. Becke, *J. Chem. Phys.* **1993**, *98*, 5648; b) P. J. Stephens, F. J. Devlin, C. F. Chablowski, M. J. Frisch, *J. Phys. Chem*. **1994,** *98*, 11623; c) R. H. Hertwig, W. Koch, *Chem. Phys. Lett*. **1997**, *268*, 345; d) S. H., Vosko, L. Wilk, M. Nusair, *Can. J. Phys.* **1980**, *58*, 1200.

[37] a) Y. Sakai, E. Miyoshi, M. Klobukowski, S. Huzinaga, *J. Chem. Phys.* **1997**, *106*, 8084; b) T. Noro, M. Sekiya, T. Koga, *Theor. Chem. Acc.* **1997**, *98*, 25; c) Y. Osanai, M. S. Mon, T. Noro, H. Mori, H. Nakashima, M. Klobukowski, E. Miyoshi, *Chem. Phys. Lett.* **2008**, *452*, 210; d) T. Noro, M. Sekiya, T. Koga, H. Matsuyama, *Theor. Chem. Acc.* **2000**, *104*, 146.

[38] a) M.W.Schmidt, K.K.Baldridge, J.A.Boatz, S.T.Elbert, M.S.Gordon, J.H.Jensen, S.Koseki, N.Matsunaga, K.A.Nguyen, S.Su, T.L.Windus, M.Dupuis, J.A.Montgomery, *J. Comput. Chem.* **1993**, *14*, 1347; b) M. S. Gordon, M. W. Schmidt pp. 1167-1189, in *"Theory and Applications of Computational Chemistry: the first forty years"* C.E.Dykstra, G.Frenking, K.S.Kim, G.E.Scuseria (editors), Elsevier, Amsterdam, **2005**.

Table 1: Comparison of observed[a] and unscaled calculated[b] vibrational frequencies [cm^{-1}] and intensities for $V(N_3)_4$.

		approx. mode description[c]	observed Raman	Calculated[d] MP2/MCP-TZP point group S_4
A	ν_1	$\nu_{as}N_3$ iph	2072 [8]	2073 (0) [711]
	ν_2	ν_sN_3 iph		1331 (0) [0.3]
	ν_3	δN_3 ipl, iph	644 [2]	620 (0) [14]
	ν_4	δN_3 ipl, iph		587 (0) [2.7]
	ν_5	νVN_4 iph	467 [10]	450 (0) [208]
	ν_6	δNVN iph		214 (0) [4.3]
	ν_7	δVNN iph		72 (0) [38]
	ν_8	δVNN oph		29 (0) [36]
B	ν_9	$\nu_{as}N_3$ oph	2072 [8]	2071 (1509) [77]
	ν_{10}	ν_sN_3 oph	[e]	1341 (296) [22]
	ν_{11}	δN_3 ipl, oph		666 (168) [1.0]
	ν_{12}	δN_3 opl, oph	579 [2]	571 (40) [16]
	ν_{13}	δN_3 opl, oph		560 (46) [7.3]
	ν_{14}	δNVN oph	223 [1]	247 (0.1) [22]
	ν_{15}	δNVN oph		162 (0.7) [5.3]
	ν_{16}	δVNN oph		32 (0.02) [25]
	ν_{17}	δVNN oph		12 (0.01) [17]
E	ν_{18}	$\nu_{as}N_3$ oph	2072 [8]	2064 (2965) [79]
	ν_{19}	ν_sN_3 oph	[e]	1336 (586) [71]
	ν_{20}	δN_3 ipl, oph		642 (371) [0.6]
	ν_{21}	δN_3 opl, oph		589 (22) [0.4]
	ν_{22}	νVN_4 oph		545 (223) [8.3]
	ν_{23}	δNVN oph		192 (6.0) [8.3]
	ν_{24}	δVNN oph		83 (0.3) [0.7]
	ν_{25}	δVNN oph		23 (0.5) [35]

[a] Spectrum recorded for the amorphous powder at -80 °C in a Teflon-FEP tube at a power level of 20 mW; on one occasion, we succeeded to record a spectrum of a crystallinic sample, before it exploded, which gave the following sharp well-resolved lines: 2094 [4.5], 2052 [3], 1309 [0.5], 655 [2], 483 [10], 434 [7.5], 383 [5.6], 105 [3]. [b] Calculated IR and Raman intensities are given in km mol^{-1} and $Å^4\,amu^{-1}$, respectively. [c] iph = in phase, oph = out of phase, ipl = in plane, opl = out of plane. [d] The vibrational spectra were also calculated in point group S_4 at the B3LYP/MCP-TZP level of theory; the results are given as Table S1 in the Supplemementary Material. [e] Hidden by bands from the Teflon-FEP sample container.

Table 2: Calculated structures[a] for $V(N_3)_4$, $[V(N_3)_6]^{2-}$ and $[V(N_3)_6]^-$

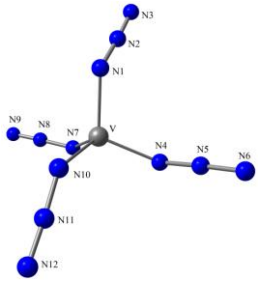

$V(N_3)_4$ D_{2d}

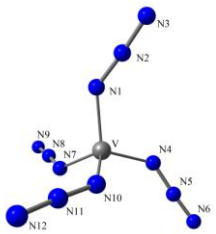

$V(N_3)_4$ S_4

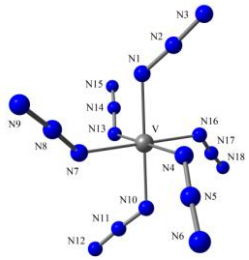

$V(N_3)_6^{2-}$ C_i

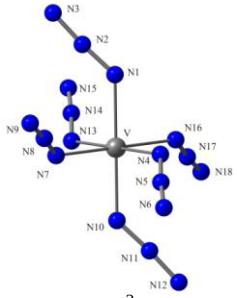

$V(N_3)_6^{2-}$ D_{3d}

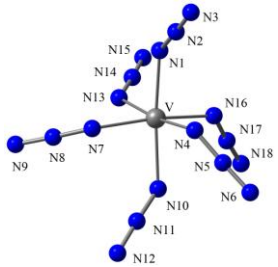

$V(N_3)_6^-$ C_1

	$V(N_3)_4$ D_{2d}	$V(N_3)_4$ S_4	$V(N_3)_6^{2-}$ C_i		$V(N_3)_6^{2-}$ D_{3d}		$V(N_3)_6^-$ C_1
	B3LYP	MP2	B3LYP	MP2	B3LYP	MP2	B3LYP
V-N	1.870	1.841	2.024 (ax) 2.029 (eq)	2.005	2.026	2.005	1.945(N7), 1.951(N1), 1.952(N16) 1.986(N13), 1.987(N10), 1.988(N4)
N1-N2	1.220	1.212	1.191	1.199	1.189	1.198	1.197
N2-N3	1.122	1.159	1.142	1.176	1.145	1.177	1.133
N4-N5	1.220	1.212	1.188	1.197	1.189	1.198	1.199
N5-N6	1.122	1.159	1.144	1.176	1.145	1.177	1.134
N7-N8	1.220	1.212	1.188	1.197	1.189	1.198	1.198
N8-N9	1.122	1.159	1.144	1.176	1.145	1.177	1.133
N10-N11	1.220	1.212	1.191	1.199	1.189	1.198	1.199
N11-N12	1.122	1.159	1.142	1.176	1.145	1.177	1.134
N13-N14	-	-	1.188	1.197	1.189	1.198	1.198
N14-N15	-	-	1.144	1.176	1.145	1.177	1.135
N16-N17	-	-	1.188	1.197	1.189	1.198	1.199
N17-N18	-	-	1.144	1.176	1.145	1.177	1.133
N1-V-N4	111.5	110.3	89.6	89.7	89.2	89.6	83.0
N1-V-N7	111.5	110.3	90.3	90.3	90.8	90.4	93.7
N1-V-N10	105.4	107.9	180.0	180.0	180.0	180.0	170.8
N1-V-N13	-	-	90.4	90.3	90.8	90.4	90.9
N1-V-N16	-	-	89.7	89.7	89.2	89.6	96.2
N4-V-N7	105.4	107.9	90.0	89.1	90.8	90.4	97.0
N4-V-N10	111.5	110.3	90.4	90.3	90.8	90.4	87.8
N4-V-N13	-	-	180.0	180.0	180.0	180.0	173.0
N4-V-N16	-	-	90.0	90.9	89.2	89.6	92.4
N7-V-N10	111.5	110.3	89.7	89.7	89.2	89.6	87.1
N7-V-N13	-	-	90.0	90.9	89.2	89.6	84.8
N7-V-N16	-	-	180.0	180.0	180.0	180.0	167.5
N10-V-N13	-	-	89.6	89.7	89.2	89.6	98.3
N10-V-N16	-	-	90.3	90.3	90.8	90.4	84.5
N13-V-N16	-	-	90.0	89.1	90.8	90.4	86.8
V-N-N	132.1	136.1	129.2 (ax) 132.1 (eq)	129.6 (ax) 132.1 (eq)	134.9	133.5	128.5(N4), 129.2(N10), 130.4(N13), 131.7(N16), 132.5(N7), 133.0(N1)
N-N-N	175.2	176.2	176.5 (ax) 176.6 (eq)	176.5 (ax) 176.6 (eq)	176.3	176.5	177.0(N10), 177.1(N4), 177.1(N16) 177.1(N7), 177.2(N14), 177.4(N1)

[a] Calculated at the B3LYP/MCP-TZP and MP2/MCP-TZP levels of theory. Bond lengths in [Å] and angles in [°].

Table 3: Comparison of observed[a] and unscaled calculated[b] vibrational frequencies [cm^{-1}] and intensities for $[V(N_3)_6]^-$ in point group C_1.

Approx mode description in C_1[c]		Observed Ra	Calculated[b] B3LYP/MCP-TZP
ν_1	$\nu_{as}N_3$ iph	2112 [10.0]	2159 (129) [874]
ν_2	$\nu_{as}N_3$ oph		2134 (1645) [181]
ν_3	$\nu_{as}N_3$ oph	2079 [5.1]	2126 (1463) [231]
ν_4	$\nu_{as}N_3$ oph		2118 (2156) [58]
ν_5	$\nu_{as}N_3$ oph	2047 [3.8]	2111 (52) [226]
ν_6	$\nu_{as}N_3$ oph	2027 [1.1]	2102 (313) [156]
ν_7	ν_sN_3 iph	1378 [1][d]	1378 (7.3) [3.4]
ν_8	ν_sN_3 oph		1361 (288) [0.8]
ν_9	ν_sN_3 oph	1342 [1.3]	1358 (301) [3.4]
ν_{10}	ν_sN_3 oph		1354 (48) [2.6]
ν_{11}	ν_sN_3 oph		1347 (330) [2.0]
ν_{12}	ν_sN_3 oph		1346 (215) [1.8]
ν_{13}	δN_3		664 (3.2) [0.6]
ν_{14}	δN_3		653 (25) [0.8]
ν_{15}	δN_3		649 (33) [0.6]
ν_{16}	δN_3		647 (8.0) [0.8]
ν_{17}	δN_3	649 [0.5]	644 (49) [3.2]
ν_{18}	δN_3		643 (36) [3.4]
ν_{19}	δN_3		625 (8.3) [1.0]
ν_{20}	δN_3		622 (6.4) [0.3]
ν_{21}	δN_3	607 [0.3]	621 (1.0) [1.7]
ν_{22}	δN_3		615 (12) [0.9]
ν_{23}	δN_3	588 [0.3]	613 (3.0) [3.1]
ν_{24}	δN_3		609 (4.7) [0.4]
ν_{25}	ν_sVN_6 oph	453 [5.8]	459 (326) [8.7]
ν_{26}	$\nu_{as}VN_6$		453 (331) [2.1]
ν_{27}	$\nu_{as}VN_6$(short T against long T)		433 (391) [1.7]
ν_{28}	ν_sVN_6 iph	420 [8.9] , 405 [6.4]	421 (1.7) [78]
ν_{29}	δVNN	366 [1.3]	336 (0.4) [1.3]
ν_{30}	δVNN		327 (3.6) [2.0]
ν_{31}	δVNN		321 (0.3) [1.9]
ν_{32}	δVNN	345 [0.7]]	307 (5.0) [7.9]
ν_{33}	δNVN		288 (7.1) [7.9]
ν_{34}	δNVN		265 (0.4) [7.1]
ν_{35}	δNVN		249 (1.4) [6.1]
ν_{36}	δNVN	265 [0.6]	230 (0.7) [13]
ν_{37}	δ_{sciss}NVN		191 (1.3) [12]
ν_{38}	$\delta_{twist}VN_4$		173 (2.2) [9.1]
ν_{39}	$\delta_{twist}VN_4$		164 (0.6) [16]
ν_{40}	$\delta_{wag}N_3$		117 (0.5) [5.5]
ν_{41}	$\delta_{wag}N_3$		106 (1.2) [2.9]
ν_{42}	$\delta_{wag}N_3$		96 (0.5) [17]
ν_{43}	$\delta_{wag}N_3$		68 (0.7) [17]
ν_{44}	$\delta_{wag}N_3$		62 (0.2) [5.1]
ν_{45}	τV-N_3		59 (0.2) [23]
ν_{46}	τV-N_3		48 (0.2) [14]
ν_{47}	τV-N_3		40 (0.06) [6.8]
ν_{48}	τV-N_3		34 (0.4) [11]
ν_{49}	τV-N_3		27 (1.7) [5.1]
ν_{50}	τV-N_3		24 (0.7) [15]
ν_{51}	τV-N_3		17 (0.3) [4.2]

[a] As $[NMe_4]^+$ salt. In addition to the bands listed in this table, the following weak Raman bands were observed: 231 [0.5], 186 [1.0], 155 [1.1] cm^{-1}. [b] Calculated at the B3LYP/MCP-TZP level; the IR and Raman intensities are given in km mol^{-1} and $Å^4$ amu^{-1}. [c] iph = in phase, oph = out of phase. [d] Intensity uncertain due to interference from a Teflon band.

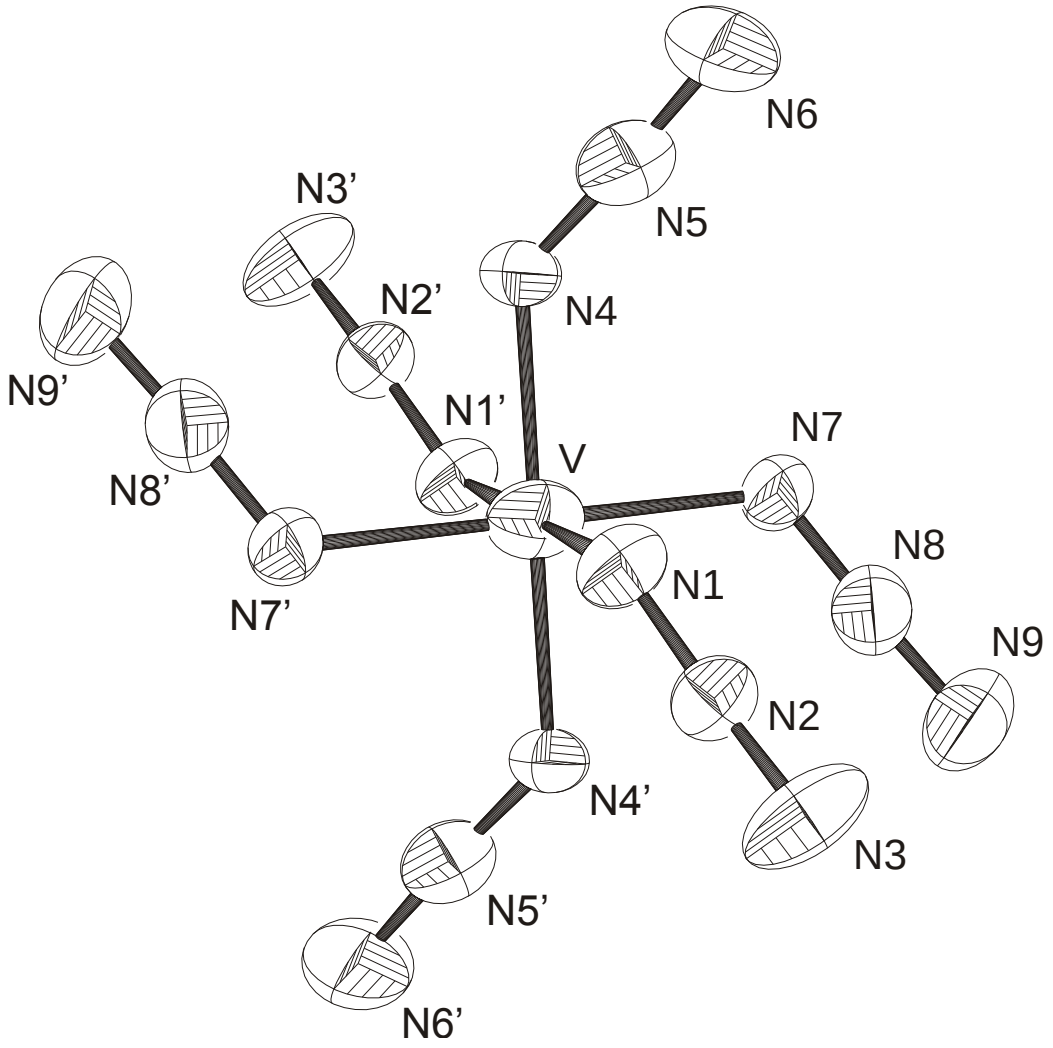

Figure 1: ORTEP drawing of the $[V(N_3)_6]^{2-}$ anion in $[PPh_4]_2[V(N_3)_6]$. Thermal ellipsoids are shown at the 50% probability level. Selected bond lengths [Å] and angles [°]: V-N1 2.017(3), V-N4 1.923(3), V-N7 2.005(3), N1-N2 1.211(4), N2-N3 1.126(40, N4-N5 1.218(5), N5-N6 1.150(6), N7-N8 !.188(4), N8-N9 1.158(5), V-N1-N2 123.6(3), V-N4-N5 133.5(3), V-N7-N8 121.9(3), N1-V-N4 89.89(13), N1-V-N4' 90.11(13), N1-V-N7 90.02(13), N1-V-N7' 89.98(13), N4-V-N4' 179.999(2), N4-V-N7 90.69(13), N4-V-N7' 89.31(13), N1-N2-N3 174.6(4), N4-N5-N6 175.0(5), N7-N8-N9 177,2(4).

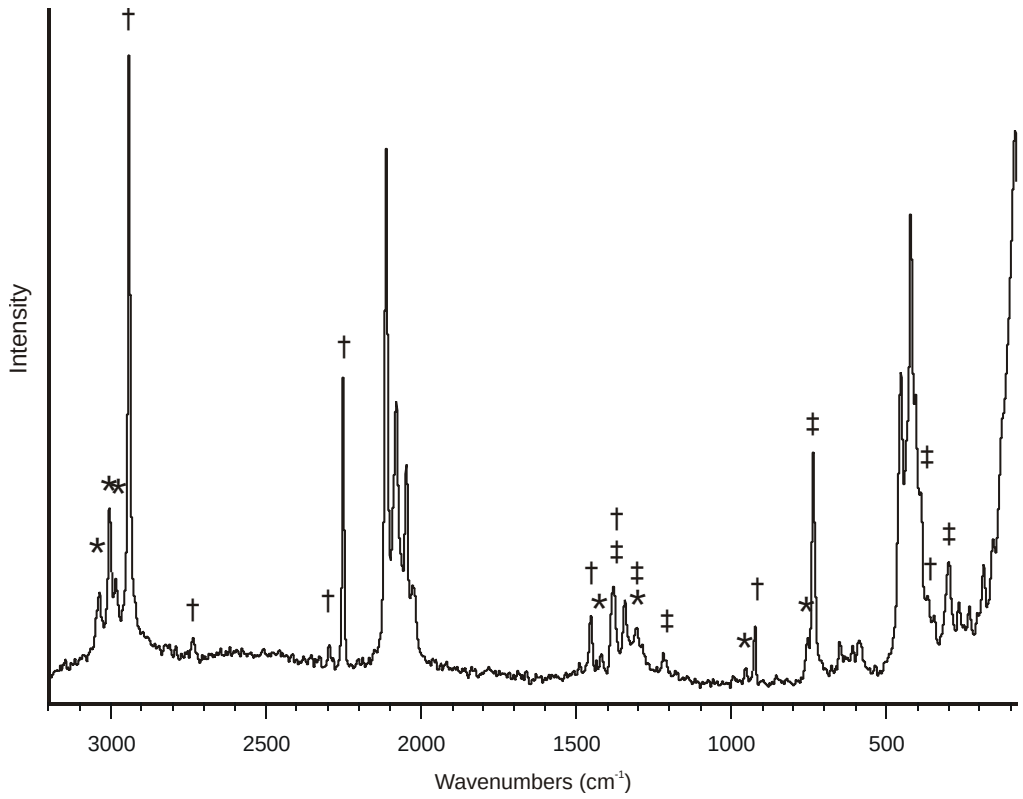

Figure 2: Low-temperature Raman spectrum of $[NMe_4][V(N_3)_6]$. Bands belonging to the NMe_4 cation are marked with an asterisk(*). Bands marked with a dagger (†) are due to a residual amount of CH_3CN solvent. Bands due to the FEP sample container are marked with a double dagger (‡).

Synopsis

Ralf Haiges*, Jerry A. Boatz, and Karl O. Christe*

The Syntheses and Structure of the First Vanadium(IV) and Vanadium(V) Binary Azides, $V(N_3)_4$, $[V(N_3)_6]^{2-}$, and $[V(N_3)_6]^-$

Shock-sensitive and explosive $V(N_3)_4$ was prepared from VF_4 and Me_3SiN_3 by fluoride-azide exchange. Substitution of VF_4 by VF_5 also produced $V(N_3)_4$ due to reduction of the metal center by the azide anion. Salts of the $[V(N_3)_6]^{2-}$ anion were obtained by treatment of the neutral tetraazide with ionic azides, and the crystal structure of $[Ph_4P]_2[V(N_3)_6]$ was determined. For the synthesis of a binary vanadium(V) azide, it was necessary to reduce the oxidizing power of VF_5 by the use of the more weakly oxidizing VF_6^- anion. This approach permitted the successful synthesis of the $[V(N_3)_6]^-$ anion, the only binary vanadium(V) compound known besides VF_5, VF_6^- and V_2O_5.

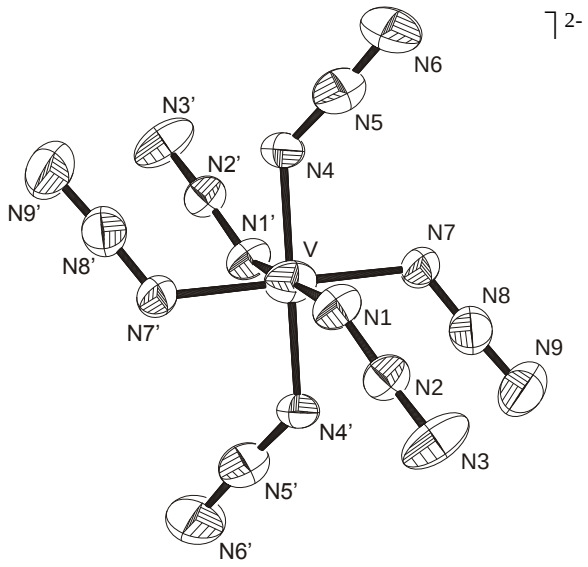

The Syntheses and Structure of the First Vanadium(IV) and Vanadium(V) Binary Azides, $V(N_3)_4$, $[V(N_3)_6]^{2-}$ and $[V(N_3)_6]^-$

Ralf Haiges, Jerry A. Boatz, and Karl O. Christe**

Supplementary Information

Table S1: Vibrational spectrum of $V(N_3)_4$ calculated at the B3LYP/MCP-TZP level of theory.

Table S2: Comparison of observed and unscaled calculated vibrational frequencies and intensities for $[V(N_3)_6]^{2-}$ in point group C_i.

Table S3: Unscaled calculated vibrational frequencies and intensities for $[V(N_3)_6]^{2-}$ in point group D_{3d}.

Table S4: Structure refinement data for $[Ph_4P]_2[V(N_3)_6]$.

Table S5: Atomic coordinates and equivalent isotropic displacement parameters for $[Ph_4P]_2[V(N_3)_6]$.

Table S6: Bond lengths and angles for $[Ph_4P]_2[V(N_3)_6]$.

Table S7: Anisotropic displacement parameters for $[Ph_4P]_2[V(N_3)_6]$.

Table S8: Hydrogen coordinates and isotropic displacement parameters for $[Ph_4P]_2[V(N_3)_6]$.

Figure S1: IR (top) and Raman (bottom) spectra of $[PPh_4]_2[V(N_3)_6]$.

Table S1: Unscaled vibrational frequencies [cm^{-1}] and intensities[a] for $V(N_3)_4$ calculated at the B3LYP/MCP-TZP level of theory.

	approx. mode description[b]	B3LYP/MCP-TZP point group D_{2d}	
ν_1	$\nu_{as}N_3$ iph	A_1	2194 (0) [710]
ν_2	ν_sN_3 iph	A_1	1323 (0) [3.1]
ν_3	δN_3 ipl, iph	A_1	649 (0) [3.0]
ν_4	δN_3 ipl, iph	A_2	602 (0) [0]
ν_5	νVN_4 iph	A_1	450 (0) [53]
ν_6	δNVN iph	A_1	183 (0) [38]
ν_7	δVNN iph	A_2	102 (0) [0]
ν_8	δVNN oph	A_1	44 (0) [3.7]
ν_9	$\nu_{as}N_3$ oph	B_2	2160 (28) [381]
ν_{10}	ν_sN_3 oph	B_2	1298 (55) [0.1]
ν_{11}	δN_3 ipl, oph	B_2	649 (113) [0.3]
ν_{12}	δN_3 opl, oph	B_1	597 (0) [0.01]
ν_{13}	δN_3 opl, oph	B_2	513 (66) [5.0]
ν_{14}	δNVN oph	B_1	154 (0) [6.2]
ν_{15}	δNVN oph	B_2	139 (3.1) [16]
ν_{16}	δVNN oph	B_2	63 (1.1) [0.4]
ν_{17}	δVNN oph	B_1	37 (0) [30]
ν_{18}	$\nu_{as}N_3$ oph	E	2167 (3345) [16]
ν_{19}	ν_sN_3 oph	E	1303 (1462) [0.7]
ν_{20}	δN_3 ipl, oph	E	653 (120) [0.4]
ν_{21}	δN_3 opl, oph	E	606 (73) [1.0]
ν_{22}	νVN_4 oph	E	541 (280) [0.1]
ν_{23}	δNVN oph	E	241 (3.9) [5.8]
ν_{24}	δVNN oph	E	94 (3.8) [14]
ν_{25}	δVNN oph	E	38 (0.01) [8.6]

[a] Calculated IR and Raman intensities are given in km mol^{-1} and $Å^4$ amu^{-1}, respectively. [b] iph = in phase, oph = out of phase, ipl = in plane, opl = out of plane.

Table S2: Comparison of observed[a] and unscaled calculated[b] vibrational frequencies [cm^{-1}] and intensities for $[V(N_3)_6]^{2-}$ in point group C_i.

	approx. mode description in C_i[c]		observed		calculated[b] (IR) [Raman]	
			IR	Ra	B3LYP/MCP-TZP	MP2/MCP-TZP
A_g	ν_1	$\nu_{as}N_3$(eq) oph		2079 [10.0]	2154 (0) [807]	2189 (0) [91]
	ν_2	$\nu_{as}N_3$ eq iph, ax oph		2041 [0.4]	2111 (0) [246]	2186 (0) [94]
	ν_3	$\nu_{as}N_3$ iph		2020 [0.4]	2097 (0) [179]	2172 (0) [880]
	ν_4	ν_sN_3(eq) iph		1341 [0.1]	1386 (0) [31]	1303 (0) [98]
	ν_5	ν_sN_3(eq) oph		1330 [0.1]	1375 (0) [46]	1301 (0) [148]
	ν_6	ν_sN_3(ax) iph		1315 [0.2]	1368 (0) [30]	1298 (0) [123]
	ν_7	δN_3 ipl, iph		651 [0.1]	676 (0) [1.5]	656 (0) [3.2]
	ν_8	δN_3 ipl, oph		639 [0.1]	668 (0) [1.7]	649 (0) [8.2]
	ν_9	δN_3(eq) ipl, oph		628 [0.05]	661 (0) [2.9]	643 (0) [10]
	ν_{10}	δN_3 opl, iph		591 [0.1]	634 (0) [0.2]	598 (0) [2.0]
	ν_{11}	δN_3(eq) opl, oph			629 (0) [1.2]	592 (0) [0.9]
	ν_{12}	δN_3 opl, oph		583 [0.1]	623 (0) [3.0]	589 (0) [5.9]
	ν_{13}	νVN_6 iph		401 [5.0]	380 (0) [79]	400 (0) [215]
	ν_{14}	νVN_6 oph		326 [0.4]	317 (0) [8.3]	343 (0) [70]
	ν_{15}	νVN_4(eq) oph		293 [0.1]	290 (0) [8.0]	327 (0) [65]
	ν_{16}	$\delta N_{ax}VN_{eq}$ oph		247 [0.1]	245 (0) [11]	235 (0) [18]
	ν_{17}	$\delta N_{ax}VN_{eq}$ oph		235 [0.05]	227 (0) [9.7]	232 (0) [12]
	ν_{18}	$\delta N_{ax}VN_{eq}$ oph		207 [0.7]	200 (0) [29]	199 (0) [30]
	ν_{19}	δVNN ipl, iph		115 [2.3]	102 (0) [40]	74 (0) [53]
	ν_{20}	δVNN_{eq} ipl, oph		94 [2.5]	91 (0) [16]	71 (0) [25]
	ν_{21}	δVNN_{eq} opl, oph			51 (0) [30]	65 (0) [0.1]
	ν_{22}	δVNN ipl, oph			51 (0) [4.1]	38 (0) [33]
	ν_{23}	δVNN_{eq} ipl, iph			33 (0) [27]	29 (0) [28]
	ν_{24}	δVNN_{ax} opl, iph			29 (0) [30]	29 (0) [32]
A_u	ν_{25}	$\nu_{as}N_3$(eq) oph	2036 vs		2114 (3058) [0]	2189 (2373) [0]
	ν_{26}	$\nu_{as}N_3$ oph	2021 sh		2112 (2932) [0]	2174 (1969) [0]
	ν_{27}	$\nu_{as}N_3$ oph	1998 sh		2107 (1919) [0]	2169 (1221) [0]
	ν_{28}	ν_sN_3(eq) oph	1331 ms		1374 (209) [0]	1303 (85) [0]
	ν_{29}	ν_sN_3(eq) oph	1320 ms		1371 (306) [0]	1299 (173) [0]
	ν_{30}	ν_sN_3(ax) oph	1312 ms		1362 (301) [0]	1298 (138) [0]
	ν_{31}	δN_3(eq) ipl, oph	650 sh		676 (40) [0]	656 (53) [0]
	ν_{32}	δN_3(eq) ipl, oph	637 mw		664 (55) [0]	648 (36) [0]
	ν_{33}	δN_3(eq) ipl, oph			663 (14) [0]	647 (59) [0]
	ν_{34}	δN_3 opl, oph	597 sh		640 (15) [0]	603 (10) [0]
	ν_{35}	δN_3(ax) ipl, oph	592 w		636 (10) [0]	602 (6.7) [0]
	ν_{36}	δN_3(ax) ipl, oph			635 (9.1) [0]	601 (1.6) [0]
	ν_{37}	νVN_4(eq) oph			407 (425) [0]	433 (806) [0]
	ν_{38}	νVN_2(ax) oph	407 s		389 (553) [0]	430 (608) [0]
	ν_{39}	νVN_4(eq) oph			381 (398) [0]	409 (508) [0]
	ν_{40}	$\delta N_{eq}VN_{eq}$ ipl, oph			278 (9.7) [0]	281 (13) [0]
	ν_{41}	$\delta N_{ax}VN_{eq}$ iph			250 (12) [0]	244 (12) [0]
	ν_{42}	$\delta N_{ax}VN_{ax}$			230 (18) [0]	220 (17) [0]
	ν_{43}	δNVN iph			172 (2.6) [0]	171 (2.2) [0]
	ν_{44}	$\delta N_{eq}VN_{eq}$ opl, oph			154 (8.9) [0]	156 (9.8) [0]
	ν_{45}	$\delta N_{eq}VN_{eq}$ ipl, oph			154 (3.9) [0]	139 (3.6) [0]
	ν_{46}	δVNN ipl, oph			59 (4.1) [0]	46 (8.2) [0]
	ν_{47}	δVNN ipl, oph			52 (2.3) [0]	40 (3.2) [0]
	ν_{48}	δVNN_{eq} opl, iph			44 (0.8) [0]	33 (2.3) [0]
	ν_{49}	δVNN opl, oph			34 (1.3) [0]	27 (1.0) [0]
	ν_{50}	δVNN opl, oph			24 (2.1) [0]	27 (0.4) [0]
	ν_{51}	δVNN			22 (0.01) [0]	20 (0.005) [0]

[a] As $[PPh_4]^+$ salt. In addition to the bands listed in this table, the following bands due to the cation were observed: Raman, 3068 [2.2], 2938 [0.2], 1586 [1.0], 1577 [0.3], 1182 [0.3], 1163 [0.3], 1111 [0.3], 1099 [0.7], 1027 [0.9], 1000 [1.5], 680 [0.4], 616 [0.4], 255 [0.4]; IR, 3060 vw, 1585 mw, 1482 mw, 1436 m, 1277 vw, 1188 w, 1158 w, 1109 ms, 1027 vw, 996 mw, 854 vw, 758 w, 753 ms, 692 ms, 615 vw, 528 s. [b] Calculated at the B3LYP/MCP-TZP and MP2/MCP-TZP levels of theory. IR and Raman intensities are given in km mol^{-1} and $Å^4$ amu^{-1}, respectively. [c] ax = axial, eq = equatorial, ipl = in plane, opl = out of plane, iph = in phase, oph = out of phase.

Table S3: Unscaled calculated[a] vibrational frequencies [cm^{-1}] and intensities for $[V(N_3)_6]^{2-}$ in point group D_{3d}.

		approx. mode description in D_{3d}[b]	Calculated (IR) [Raman] B3LYP/MCP-TZP	MP2/MCP-TZP
A_{1g}	ν_1	$\nu_{as}N_3$ iph	2160 (0) [897]	2172 (0) [1110]
	ν_2	ν_sN_3 iph	1389 (0) [39]	1298 (0) [59]
	ν_3	δN_3 ipl, iph	668 (0) [0.8]	650 (0) [0.8]
	ν_4	νVN_6 iph	376 (0) [86]	401 (0) [193]
	ν_5	$\delta N_{ax}VN_{eq}$ iph	207 (0) [49]	198 (0) [80]
	ν_6	δVNN ipl, iph	44 (0) [12]	35 (0) [12]
A_{2g}	ν_7	δN_3 opl, oph	629 (0) [0]	595 (0) [0]
	ν_8	δVNN ipl, iph	38 (0) [0]	74 (0) [0]
E_g	ν_9	$\nu_{as}N_3$ (eq) oph	2091 (0) [321]	2188 (0) [165]
	ν_{10}	ν_sN_3 oph	1375 (0) [70]	1296 (0) [256]
	ν_{11}	δN_3 ipl, oph	658 (0) [1.1]	640 (0) [11]
	ν_{12}	δN_3 opl, oph	630 (0) [1.2]	591 (0) [6.3]
	ν_{13}	νVN_6 oph	288 (0) [19]	326 (0) [122]
	ν_{14}	δNVN	228 (0) [0.5]	225 (0) [1.2]
	ν_{15}	δVNN ipl, oph	77 (0) [62]	70 (0) [69]
	ν_{16}	δVNN opl, oph	45 (0) [44]	37 (0) [40]
A_{1u}	ν_{17}	δN_3 opl, oph	636 (0) [0]	600 (0) [0]
	ν_{18}	$\delta N_{ax}VN_{eq}$ oph	189 (0) [0]	202 (0) [0]
	ν_{19}	δVNN opl, oph	45 (0) [0]	31 (0) [0]
A_{2u}	ν_{20}	$\nu_{as}N_3$ oph	2088 (70) [0]	2158 (79) [0]
	ν_{21}	ν_sN_3 oph	1376 (29) [0]	1300 (36) [0]
	ν_{22}	δN_3 ipl, oph	660 (78) [0]	644 (69) [0]
	ν_{23}	νVN_6 oph	376 (196) [0]	402 (236) [0]
	ν_{24}	$\delta N_{ax}VN_{eq}$ oph	179 (0.1) [0]	176 (0.3) [0]
	ν_{25}	δVNN ipl, oph	63 (8.0) [0]	57 (10) [0]
E_u	ν_{26}	$\nu_{as}N_3$ oph	2116 (7416) [0]	2187 (4821) [0]
	ν_{27}	ν_sN_3 oph	1371 (774) [0]	1294 (373) [0]
	ν_{28}	δN_3 (eq) ipl, oph	661 (4.7) [0]	644 (61) [0]
	ν_{29}	δN_3 opl, oph	634 (34) [0]	599 (20) [0]
	ν_{30}	νVN_6 oph	386 (1249) [0]	428 (1697) [0]
	ν_{31}	δNVN	286 (11) [0]	283 (34) [0]
	ν_{32}	δNVN	137 (5.8) [0]	131 (7.8) [0]
	ν_{33}	δVNN ipl/opl, oph	40 (0.6) [0]	36 (4.7) [0]
	ν_{34}	δVNN ipl/opl, oph	29 (4.1) [0]	30 (1.5) [0]

[a] Calculated IR and Raman intensities are given in km mol^{-1} and $Å^4\,amu^{-1}$, respectively. [b] ax = axial, eq = equatorial, ipl = in plane, opl = out of plane, iph = in phase, oph = out of phase.

Table S4: Structure refinement data for $[Ph_4P]_2[V(N_3)_6]$.

empirical formula	$C_{48}H_{40}N_{18}P_2V$
formula weight	981.86
Temperature, K	143(2)
crystal system	triclinic
space group	*P*-1
a, Å	10.098(3)
b, Å	10.365(3)
c, Å	12.258(4)
α, °	88.498(6)
β, °	75.688(6)
γ, °	69.406(6)
V, Å^3	1161.1(7)
Z	1
ρ_{calc} g/cm^3	1.404
F(000)	507
Index ranges	$-13 \leq h \leq 13, -12 \leq k \leq 13, -13 \leq l \leq 15$
μ, mm^{-1}	0.340
crystal size, mm	0.28 x 0.20 x 0.05
λ, Å	0.71073
no. of rflns. collect.	7186
no. of indep. rflns.	5017
R_{int}	0.0241
no. of params.	313
*R*1, *wR*2 [I>2σ(I)]	0.0666, 0.1757
*R*1, *wR*2 (all data)	0.0955, 0.1938
$(\Delta/\rho)_{min/max}$, e Å^{-3}	1.049/-0.490

Table S5: Atomic coordinates (x 10^4) and equivalent isotropic displacement parameters ($Å^2$x 10^3) for $[Ph_4P]_2[V(N_3)_6]$. U(eq) is defined as one third of the trace of the orthogonalized U^{ij} tensor.

	x	y	z	U(eq)
V(1)	0	10000	5000	47(1)
P(1)	1915(1)	3900(1)	1806(1)	27(1)
N(1)	-402(3)	9383(3)	6583(3)	44(1)
N(2)	493(3)	9050(3)	7136(3)	39(1)
N(3)	1237(4)	8751(5)	7722(3)	64(1)
N(4)	2054(3)	8978(3)	4797(3)	42(1)
N(5)	2961(4)	8085(4)	4101(4)	59(1)
N(6)	3849(5)	7189(6)	3508(5)	103(2)
N(7)	-274(4)	8345(3)	4419(3)	42(1)
N(8)	-1303(4)	8445(3)	4072(3)	50(1)
N(9)	-2287(5)	8484(4)	3731(4)	78(1)
C(1)	64(3)	4439(3)	2649(3)	28(1)
C(2)	-1034(4)	5324(4)	2194(3)	37(1)
C(3)	-2478(4)	5754(4)	2820(3)	41(1)
C(4)	-2821(4)	5317(4)	3889(3)	37(1)
C(5)	-1732(4)	4445(4)	4337(3)	39(1)
C(6)	-294(4)	3998(3)	3724(3)	32(1)
C(7)	2216(3)	2682(3)	674(3)	30(1)
C(8)	3637(4)	2062(4)	4(3)	43(1)
C(9)	3906(4)	1181(4)	-911(3)	46(1)
C(10)	2784(4)	892(4)	-1155(3)	40(1)
C(11)	1382(4)	1477(4)	-482(3)	40(1)
C(12)	1080(4)	2379(3)	435(3)	32(1)
C(13)	3188(3)	3087(3)	2623(3)	28(1)
C(14)	4146(4)	3679(4)	2841(3)	34(1)
C(15)	5155(4)	2965(4)	3430(3)	39(1)
C(16)	5213(4)	1690(4)	3806(3)	40(1)
C(17)	4256(4)	1102(4)	3608(3)	39(1)
C(18)	3242(4)	1790(3)	3008(3)	34(1)
C(19)	2207(3)	5409(3)	1221(3)	31(1)

C(20)	1875(4)	6543(4)	1955(3)	41(1)
C(21)	2056(4)	7736(4)	1536(4)	53(1)
C(22)	2545(4)	7809(5)	398(5)	61(1)
C(23)	2852(4)	6702(5)	-346(4)	58(1)
C(24)	2696(4)	5496(4)	60(3)	41(1)

Table S6: Bond lengths [Å] and angles [°] for $[Ph_4P]_2[V(N_3)_6]$.

V(1)-N(4)	1.923(3)
V(1)-N(4)#1	1.923(3)
V(1)-N(7)#1	2.005(3)
V(1)-N(7)	2.005(3)
V(1)-N(1)#1	2.017(3)
V(1)-N(1)	2.017(3)
P(1)-C(13)	1.787(3)
P(1)-C(19)	1.791(3)
P(1)-C(1)	1.793(3)
P(1)-C(7)	1.795(3)
N(1)-N(2)	1.211(4)
N(2)-N(3)	1.126(4)
N(4)-N(5)	1.218(5)
N(5)-N(6)	1.150(6)
N(7)-N(8)	1.188(4)
N(8)-N(9)	1.158(5)
C(1)-C(6)	1.388(4)
C(1)-C(2)	1.394(4)
C(2)-C(3)	1.386(5)
C(3)-C(4)	1.377(5)
C(4)-C(5)	1.379(5)
C(5)-C(6)	1.376(5)
C(7)-C(12)	1.388(5)
C(7)-C(8)	1.393(5)
C(8)-C(9)	1.377(5)
C(9)-C(10)	1.369(6)
C(10)-C(11)	1.377(5)
C(11)-C(12)	1.384(5)
C(13)-C(14)	1.392(5)
C(13)-C(18)	1.401(5)
C(14)-C(15)	1.383(5)
C(15)-C(16)	1.375(5)
C(16)-C(17)	1.380(5)
C(17)-C(18)	1.389(4)

C(19)-C(20)	1.390(5)
C(19)-C(24)	1.398(5)
C(20)-C(21)	1.380(5)
C(21)-C(22)	1.370(7)
C(22)-C(23)	1.381(7)
C(23)-C(24)	1.379(6)

N(4)-V(1)-N(4)#1	179.999(2)
N(4)-V(1)-N(7)#1	89.31(13)
N(4)#1-V(1)-N(7)#1	90.69(13)
N(4)-V(1)-N(7)	90.69(13)
N(4)#1-V(1)-N(7)	89.31(13)
N(7)#1-V(1)-N(7)	180.0
N(4)-V(1)-N(1)#1	90.11(13)
N(4)#1-V(1)-N(1)#1	89.89(13)
N(7)#1-V(1)-N(1)#1	90.02(13)
N(7)-V(1)-N(1)#1	89.98(13)
N(4)-V(1)-N(1)	89.89(13)
N(4)#1-V(1)-N(1)	90.11(13)
N(7)#1-V(1)-N(1)	89.98(13)
N(7)-V(1)-N(1)	90.02(13)
N(1)#1-V(1)-N(1)	180.0
C(13)-P(1)-C(19)	110.76(15)
C(13)-P(1)-C(1)	111.49(14)
C(19)-P(1)-C(1)	107.21(14)
C(13)-P(1)-C(7)	107.50(15)
C(19)-P(1)-C(7)	108.90(16)
C(1)-P(1)-C(7)	110.98(15)
N(2)-N(1)-V(1)	123.6(3)
N(3)-N(2)-N(1)	174.6(4)
N(5)-N(4)-V(1)	133.5(3)
N(6)-N(5)-N(4)	175.0(5)
N(8)-N(7)-V(1)	121.9(3)
N(9)-N(8)-N(7)	177.2(4)
C(6)-C(1)-C(2)	119.9(3)
C(6)-C(1)-P(1)	122.0(2)

C(2)-C(1)-P(1)	118.1(2)
C(3)-C(2)-C(1)	119.6(3)
C(4)-C(3)-C(2)	120.0(3)
C(3)-C(4)-C(5)	120.1(3)
C(6)-C(5)-C(4)	120.6(3)
C(5)-C(6)-C(1)	119.7(3)
C(12)-C(7)-C(8)	119.8(3)
C(12)-C(7)-P(1)	122.1(3)
C(8)-C(7)-P(1)	118.1(3)
C(9)-C(8)-C(7)	120.1(4)
C(10)-C(9)-C(8)	120.2(4)
C(9)-C(10)-C(11)	120.1(3)
C(10)-C(11)-C(12)	120.9(3)
C(11)-C(12)-C(7)	118.9(3)
C(14)-C(13)-C(18)	120.1(3)
C(14)-C(13)-P(1)	122.0(3)
C(18)-C(13)-P(1)	117.8(2)
C(15)-C(14)-C(13)	119.2(3)
C(16)-C(15)-C(14)	120.8(3)
C(15)-C(16)-C(17)	120.5(3)
C(16)-C(17)-C(18)	119.9(3)
C(17)-C(18)-C(13)	119.5(3)
C(20)-C(19)-C(24)	119.6(3)
C(20)-C(19)-P(1)	118.1(3)
C(24)-C(19)-P(1)	122.3(3)
C(21)-C(20)-C(19)	119.9(4)
C(22)-C(21)-C(20)	120.1(4)
C(21)-C(22)-C(23)	120.8(4)
C(24)-C(23)-C(22)	119.8(4)
C(23)-C(24)-C(19)	119.8(4)

Symmetry transformations used to generate equivalent atoms:

#1 -x,-y+2,-z+1

Table S7: Anisotropic displacement parameters ($Å^2 x\ 10^3$) for $[Ph_4P]_2[V(N_3)_6]$. The anisotropic displacement factor exponent takes the form: $-2\pi^2[\ h^2\ a^{*2}U^{11} + ...\ + 2\ h\ k\ a^*\ b^*\ U^{12}\ ]$

	U^{11}	U^{22}	U^{33}	U^{23}	U^{13}	U^{12}
V(1)	47(1)	52(1)	36(1)	15(1)	-15(1)	-10(1)
P(1)	25(1)	27(1)	24(1)	3(1)	-7(1)	-5(1)
N(1)	41(2)	53(2)	41(2)	8(2)	-17(1)	-18(2)
N(2)	43(2)	42(2)	36(2)	11(1)	-14(1)	-18(1)
N(3)	56(2)	103(3)	51(2)	38(2)	-32(2)	-40(2)
N(4)	32(2)	41(2)	44(2)	-4(2)	-13(1)	-1(1)
N(5)	42(2)	65(2)	72(3)	2(2)	-20(2)	-18(2)
N(6)	49(3)	112(4)	111(4)	-55(4)	-16(3)	16(3)
N(7)	47(2)	36(2)	47(2)	3(1)	-25(2)	-12(1)
N(8)	60(2)	45(2)	49(2)	2(2)	-20(2)	-18(2)
N(9)	88(3)	68(3)	99(4)	4(2)	-59(3)	-28(2)
C(1)	25(2)	27(2)	26(2)	2(1)	-6(1)	-5(1)
C(2)	32(2)	42(2)	30(2)	8(2)	-5(1)	-5(2)
C(3)	31(2)	42(2)	41(2)	5(2)	-9(2)	-1(2)
C(4)	28(2)	38(2)	37(2)	-7(2)	1(1)	-6(2)
C(5)	40(2)	40(2)	28(2)	6(2)	1(2)	-8(2)
C(6)	34(2)	29(2)	27(2)	5(1)	-8(1)	-6(1)
C(7)	28(2)	30(2)	25(2)	2(1)	-7(1)	-2(1)
C(8)	29(2)	48(2)	43(2)	-8(2)	-7(2)	-5(2)
C(9)	40(2)	45(2)	41(2)	-10(2)	-8(2)	-1(2)
C(10)	54(2)	30(2)	33(2)	0(1)	-16(2)	-7(2)
C(11)	45(2)	38(2)	41(2)	3(2)	-21(2)	-14(2)
C(12)	33(2)	29(2)	36(2)	7(1)	-13(1)	-8(1)
C(13)	24(2)	31(2)	22(2)	0(1)	-4(1)	-4(1)
C(14)	31(2)	37(2)	31(2)	1(1)	-6(1)	-11(2)
C(15)	30(2)	55(2)	34(2)	-3(2)	-12(2)	-15(2)
C(16)	32(2)	51(2)	32(2)	3(2)	-15(2)	-4(2)
C(17)	35(2)	38(2)	35(2)	7(2)	-11(2)	-4(2)
C(18)	30(2)	35(2)	38(2)	4(2)	-13(1)	-8(1)
C(19)	25(2)	31(2)	33(2)	8(1)	-7(1)	-5(1)

C(20)	40(2)	33(2)	44(2)	1(2)	-8(2)	-9(2)
C(21)	44(2)	33(2)	81(3)	7(2)	-18(2)	-10(2)
C(22)	37(2)	44(2)	95(4)	36(3)	-14(2)	-11(2)
C(23)	40(2)	67(3)	55(3)	35(2)	-3(2)	-11(2)
C(24)	31(2)	46(2)	35(2)	9(2)	-4(2)	-6(2)

Table S8: Hydrogen coordinates (x 10^4) and isotropic displacement parameters ($Å^2$x 10^3) for $[Ph_4P]_2[V(N_3)_6]$.

	x	y	z	U(eq)
H(2)	-793	5631	1460	45
H(3)	-3231	6350	2511	49
H(4)	-3811	5618	4319	45
H(5)	-1977	4150	5075	47
H(6)	450	3392	4036	38
H(8)	4420	2249	178	51
H(9)	4872	772	-1374	55
H(10)	2972	287	-1790	48
H(11)	613	1259	-650	48
H(12)	110	2784	894	39
H(14)	4107	4563	2588	40
H(15)	5816	3361	3577	47
H(16)	5918	1210	4205	48
H(17)	4290	227	3882	46
H(18)	2590	1383	2860	41
H(20)	1524	6497	2743	49
H(21)	1840	8508	2038	64
H(22)	2675	8630	116	73
H(23)	3170	6771	-1135	70
H(24)	2921	4727	-447	49

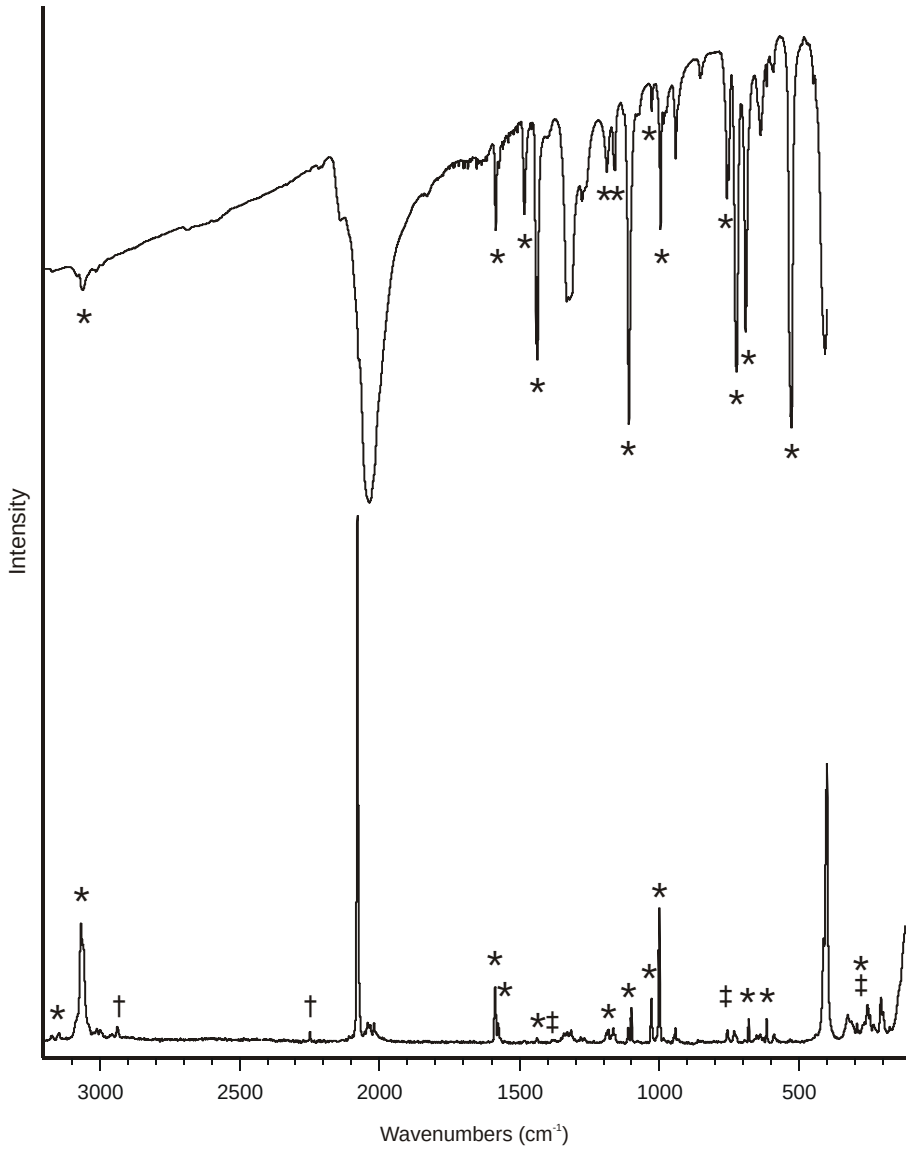

Figure S1: IR (top) and Raman (bottom) spectra of $[PPh_4]_2[V(N_3)_6]$. Bands belonging to the PPh_4 cation are marked with an asterisk(*). Bands marked with a dagger (†) are due to a residual amount of CH_3CN solvent. Bands due to the FEP sample container are marked with a double dagger (‡).